ARTICLES

Electrochemical Mass Spectroscopic and Surface Photovoltage Studies of Catalytic Water Photooxidation by Undoped and Carbon-Doped Titania

Bernhard Neumann,*,† Peter Bogdanoff,† Helmut Tributsch,† Shanmugasundaram Sakthivel,‡ and Horst Kisch‡

Department Solare Energetik, Hahn-Meitner-Institut, Glienickerstrasse 100, D-14109 Berlin, Germany, and Institut für Anorganische Chemie der Universität Erlangen-Nürnberg, Egerlandstrasse 1, D-91058 Erlangen, Germany

Received: March 15, 2005; In Final Form: June 14, 2005

Carbon-doped TiO_2, demonstrated as an efficient photocatalyst in visible light photooxidation of organic compounds, was prepared with different doping concentrations and investigated via differential electrochemical mass spectroscopy (DEMS) and capacitive surface photovoltage (SPV) measurements in the form of thin layer electrodes. In all cases the total photocurrent as well as the surface photovoltage of the doped materials decreased markedly in relation to the undoped one. No detectable oxygen evolved from the doped electrodes in acidic solution under UV-light excitation. Since an oxidation of formic acid is still apparent, it is concluded that this oxidation occurs via isolated, catalytically poorly active trap states within the forbidden energy region. The existence of these states is confirmed by capacitive SPV measurements.

Introduction

Photocatalytic activity under visible light irradiation in titanium dioxide doped by nitrogen,[1−5] carbon,[6−8] and sulfur[9−11] has been reported in the literature and has received significant attention. The potential besides self-cleaning surfaces and water purification[12] would be the use in photoelectrochemical energy conversion to produce hydrogen, the most attractive energy carrier for the future.[13]

While the ability of doped TiO_2 to improve photocatalytic activity in the form of a monitored enhanced degradation of organic molecules has been verified by different groups,[14] a systematic study of the anodic electrochemical behavior of these kinds of TiO_2 has not been yet reported. The present study is aimed at analyzing whether the electronic levels generated in the forbidden energy region of carbon-doped TiO_2 may induce oxygen evolution or if significant differences from undoped titanium dioxide will be observed. In absence of metal ions or deposited metal particles as electron drain,[15,16] thin film electrodes are necessary for such type of investigations.

The carbon-doped samples TiO_2−C1a and TiO_2−C1b were prepared by hydrolysis of titanium tetrachloride with carbon-containing bases.[6] XPS measurements of the C1s binding energies of TiO_2−C1b revealed peaks at 285.6, 287.5, and 288.5 eV. The first value arises from adventitious elemental carbon,[8] and the latter two suggest the presence of a carbonate species as also supported by the IR spectrum which exhibits low intensity peaks at 1738, 1096, and 798 cm^{-1}.[6]

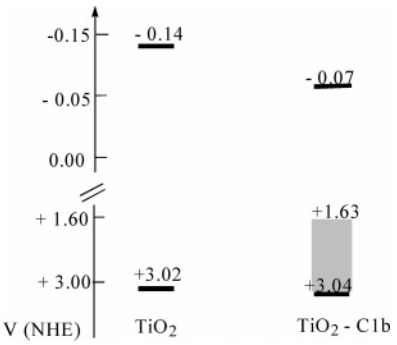

Figure 1. Band edge and surface states (dashed area) positions of undoped and doped TiO_2 at ph 0.[6]

From the pH dependence of the photovoltage, quasi-Fermi levels (electrons) at pH 7 were found to be −0.39 V and −0.48 V/NHE for TiO_2−C1a and TiO_2−C1b, respectively (Figure 1).[6,17] Wavelength-dependent photooxidation of benzoic to salicylic acid in the presence of oxygen or tetra-nitromethane as electron scavenger revealed that a broad spreading of surface states exists close to the valence band edge, as schematically depicted in Figure 1. The dashed area can be accounted as continuum and conform to the theoretical calculations of states by Asahi.[1]

Both TiO_2−C1a and TiO_2−C1b photocatalyze complete mineralization of pollutants such as 4-chlorophenol and acetaldehyde.[6] In the following we report the investigation of this material in the form of thin layer electrodes with differential electrochemical mass spectroscopy (DEMS).[18] We qualitatively evaluate interfacial reaction processes and investigate them with time- and wavelength-dependent surface photovoltage experi-

* To whom correspondence should be addressed. Tel: +049-30-8062-2508. Fax: +49−30−80262434. E-mail: bernhard.neumann@hmi.de.
† Hahn-Meitner-Institut.
‡ Universität Erlangen-Nürnberg.

10.1021/jp051339g CCC: $30.25
Published on Web 08/11/2005

ments (SPV).[19] Surface processes are studied on a nanosecond scale.

Experimental Section

The unmodified titanium dioxide P25 was purchased from Degussa (mixture of 30% rutile and 70% anatase). The brownish carbon-doped titania samples were synthesized by hydrolysis of titanium tetrachloride with tetrabutylammonium hydroxide followed by calcination at 400 °C in air.[6] Throughout this paper the samples with the highest photoactivity in degradation of 4-chlorphenol, named TiO_2−C1a (2.98 m% carbon) and TiO_2−C1b (0.42 m% carbon), were used. The mixture of TiO_2−C1a with rutile (conversion from P25, 1000 °C, 12 h, $d \sim 40$ nm) was prepared by grinding some TiO_2−C1a with rutile (15 m%) in a mortar. Doctor-blading and dip coating were used to coat thin films onto glass substrates provided with a transparent conductive oxide (F−SnO_2, 18 Ω^{-1} cm^{-1}) layer. The typical suspension for dip-coating consisted of 50 mg of TiO_2, 300 μL of ethanol (Merck, puriss.), 10 μL of acetylacetone (Fluka, >99.3%), and 8 μL of Triton X (Merck, puriss.). After the mixture was homogenized in a mortar, it was spread with a glass rod on cleaned FTO-glass (2-propanol, acetone, ultrasonic bath) fixed with Scotch tape. Film thickness ranged from 1 to 6 μm, depending on the amount of ethanol employed. Annealing in an electric furnace at 350 °C for 6 min in air finished the procedure. Using argon instead of air, led, in case of the C-doped samples, to a darker coloration with a once more reduced photoreactivity. In using dip-coating thinner films became accessible. The suspension consisted of 80 mg of TiO_2 powder, 10 mL of ethanol (Merck, puriss.), 250 μL of acetylacetone, and 150 μL of Triton X. After the mixture was homogenized for 5 min in an ultrasonic bath, the substrates were dipped with a velocity of 1 cm/minute and dried for 10 s (with a heat gun) after every dip. After finishing 10 dips, a thickness of 0.6−0.8 μm was reached, and a final heating in the furnace at 350 °C for 6 min in air followed. For optical experiments quartz glass was used as substrate.

XRD measurements were carried out with a Siemens diffractometer D500/5000 in a Bragg−Bretano geometry under Cu Kα radiation. As sample holder an (100) oriented silicon disk was used. Diffractograms were identified using the ICPDS databank and particle sizes were calculated with the Scherrer equation.

Electrochemical measurements were done in a classical three-electrode compartment, where the electrochemical cell was connected to a quadrupole mass spectrometer (Balzers, QMI 420) via a gas-porous polymer membrane (Scimat 200/40/60). A platinum wire was used as counter electrode together with a mercury-sulfate electrode as reference (0.630 V vs NHE, 25 °C, pH 1). The electrical contact was made by gluing a copper wire with silver epoxy resin onto the FTO surface, followed by a subsequent insulation with epoxy resin. The control of the electrode potential was provided by a HEKA potentiostat (scanning rate 20 mV/sec). Prior to and during all measurements, the electrolyte (0.5 M H_2SO_4, Merck) was purged with nitrogen. All investigated electrodes show a similar thickness (0.8−1 μm) and the presented cyclovoltammograms were cycled until stable courses were observed. All potentials are given with reference to the normal hydrogen electrode (NHE). The measurements with formic acid were performed with a 1 M solution dissolved in 0.5 M sulfuric acid. UV-irradiation was performed from the backside of the substrate with a 150-W xenon arc lamp in combination with a convex lens and an overall light intensity of 1.33 W/cm^2 (320−750 nm). The Vis-light source was a 250-W incandescent lamp (sodium vapor) in combination with a light guide. The final integral power intensity was determined with 36.1 mW/cm^2.

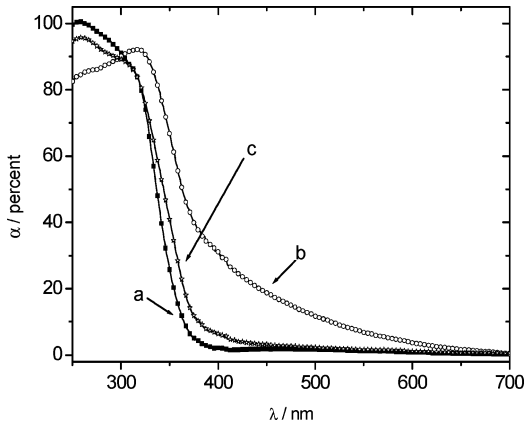

Figure 2. Absorption spectra of the thin films. The value of α was obtained by the equation $\alpha = 100 - (T + R)$, where T = transmittance (%), and R = reflectance (%). (a) pure TiO_2; (b) sample TiO_2−C1a (2.98 m% carbon); (c) sample TiO_2−C1b (0.42 m% carbon).

The time-resolved and wavelength-dependent photovoltage measurements were carried out in the arrangement of a parallel plate capacitor under the same experimental conditions as described elsewhere.[19] For excitation a pulsed N_2 laser (λ = 337 nm, duration time of the pulse 5 ns, intensity about 0.2 mJ/cm^2) was used. Spectra of the PV amplitude were measured with a 1000-W xenon lamp in combination with a quartz monochromator, providing light in the range of 0.4−4.0 eV. All investigated electrodes were similarly produced as the electrochemical working electrodes. The addition of formic acid was done by dropping 10 μL of 50% formic acid onto the TiO_2 film and waiting for dryness prior to measurement. The amount of carbon was estimated by elemental analysis.

Results and Discussion

General Investigations. According to XRD analysis all carbon-doped materials consisted of pure anatase modification (101 reflex, 12.64 °Θ; 200 reflex, 24.02 °Θ). The rather diminished signal intensity indicates amorphous areas and small crystallite sizes. Using the Scherrer equation[20] a particle size of 20 nm for P25 and 10 nm for the carbon-doped titanium dioxides could be deduced. Diffuse reflectance spectra in Figure 2 reveal that the new absorption at 400−700 nm is related to the carbon content.

The sample with the highest doping concentration shows the most pronounced shoulder and the slowest decay to zero absorption. Band gap energies of 3.02 and 3.11 eV were obtained for TiO_2−C1a and TiO_2−C1b, assuming that both are indirect semiconductors, like unmodified titania.

Electrochemical Measurements. *(a) Experimental Results.* The various titania electrodes were subjected to photocurrent measurements under positive bias coupled with in situ analysis of gaseous reaction products by mass spectroscopy. The observed current−voltage characteristics are displayed in Figure 3. All electrodes show negligible currents under darkness. Under illumination with UV-light, the undoped TiO_2 electrode (P25) shows negative currents (cathodic) from −0.05 V till +0.1 V and an onset of anodic currents above 0.1 V (0.1 mA). The signal increases with increasing voltage until a value of 0.4 mA/cm^2 at 0.3 V, where the photocurrent saturates. Applying voltages above 0.8 V led the current increases further to the maximal value of 0.75 mA/cm^2 (1.4 V).

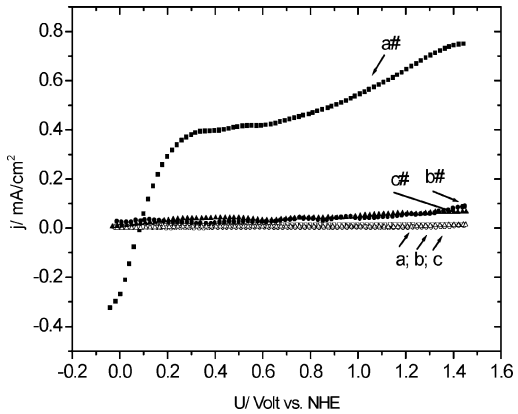

Figure 3. Darkcurrent and photocurrent density (*j*) as a function of applied potential (*U*). (a) P25; (a#) P25 UV-light; (b) TiO_2−C1a; (b#) TiO_2−C1a UV-light; (c) TiO_2−C1b; (c#) TiO_2−C1b UV-light.

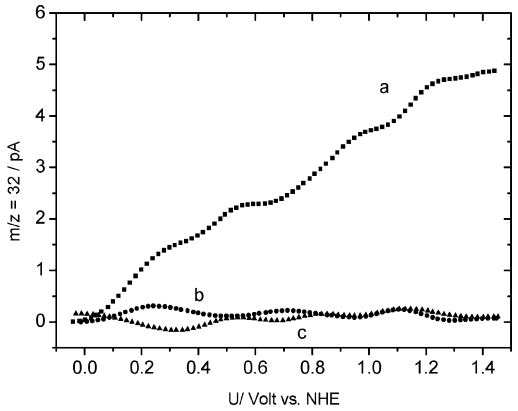

Figure 4. Dependence of photochemical oxygen evolution on an applied potential ($^{16}O_2$, *m*/*z* 32) (a) P25; (b) TiO_2−C1a; (c) TiO_2−C1b.

In comparison to the undoped material, the characteristic of the two carbon-doped electrodes (TiO_2−C1a, TiO_2−C1b) differs strongly. No cathodic currents are observed, the anodic photocurrent sets on at higher potentials 0.2 V (0.02 mA/cm^2) and the current is more then one decade lowered. At higher voltages, the signal rises up marginal to a value of about 0.06 mA/cm^2 for TiO_2−C1a and 0.08 mA/cm^2 for TiO_2−C1b (at 1.4 V/NHE). There is no significant correlation between the content of carbon and the electrochemical behavior in solely aqueous electrolyte.

Figure 4 represents the detected mass signal of oxygen ($^{16}O_2$ *m*/*z*: 32) dependent on the applied voltage. These signals were measured in situ with the current−voltage curves in Figure 3. The mass signal of the P25 electrode follows the current signal with some delay and increases linearly to a maximum value of 5 pA ($5 \cdot 10^{-12}$ A).

The different shape of the oxygen mass signal related to the photocurrent, e.g. the missed saturation-plateau, is caused by the time necessary to saturate the liquid layer (∼10 μm) between electrode and inlet system with oxygen, as well as by the high tendency of oxygen-adsorption or reaction (reduction through electrons from the conduction band-TiO_2).

The electrodes TiO_2−C1a and TiO_2−C1b show no oxygen evolution during the complete positive scan (0 pA, −0.1−1.4 V/NHE). Even though the sample was illuminated for a period of more than 20 min.

Addition of formic acid leads to an instant increase of the anodic photocurrent and to a photocurrent onset at lower voltages for all electrodes. The graphs are presented in Figure 5. The photocurrent of the P25 electrode rises up four times

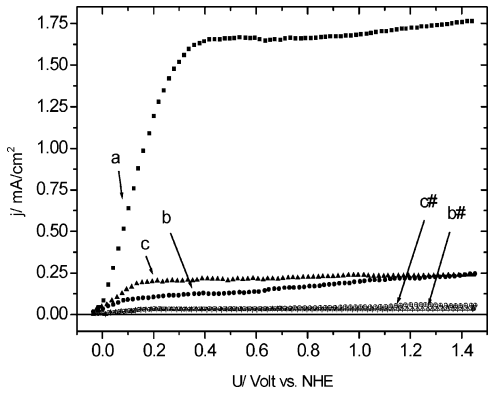

Figure 5. Photocurrent density (*j*) as a function of applied potential (*U*) under illumination (UV-light or Vis-light) in the presence of 1 M formic acid. (a) P25 UV-light; (b) TiO_2−C1a UV-light; (b#) TiO_2−C1a Vis-light; (c) TiO_2−C1b UV-light; (c#) TiO_2−C1b Vis-light.

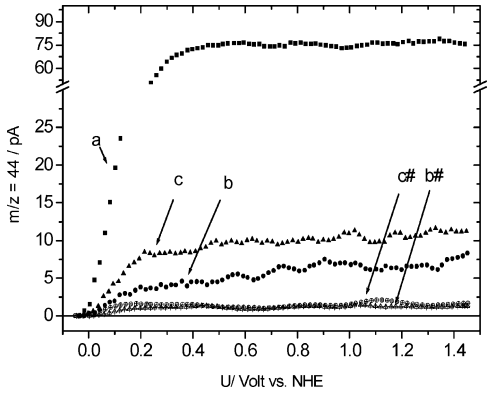

Figure 6. Dependence of photochemical carbon dioxide evolution on an applied potential ($^{12}C^{16}O_2$, *m*/*z* 44). (a) P25 UV-light; (b) TiO_2−C1a UV-light; (b#) TiO_2−C1a Vis-light; (c) TiO_2−C1b UV-light; (c#) TiO_2−C1b Vis-light. Note the much higher activity of P25 and the break in the *y*-axis.

with respect to the watersplitting reaction. The current increases from a value about 0.4 to 1.64 mA/cm^2 at 0.4 V. The carbon-doped electrodes show a similar increased photocurrent. The photocurrent of the TiO_2−C1a electrode increases from 0.04to 0.11 mA/cm^2 (0.4 V), while the photocurrent from the TiO_2−C1b electrode increases more strongly from about 0.04to 0.21 mA/cm^2 (0.4 V).

It can be concluded that for the oxidation of formic acid the sample with the lower content of carbon shows the higher activity of degradation under UV-illumination. Altogether the currents are smaller by the factor of 8 as compared to those of P25.

The excitation with light from an incandescent lamp (sodium) shows no photocurrent for the P25 electrode and marginal photocurrents for the C-doped electrodes only (TiO_2−C1a 0.015 mA/cm^2, TiO_2−C1b 0.018 mA/cm^2 at 0.4 V). Under these conditions the content of carbon at the C−TiO_2 electrodes is beneficial for the observed photocurrent.

Figure 6 represents the in situ detected mass signal of evolved carbon dioxide dependent on the applied voltage under UV- and Vis-illumination.

Under UV-illumination, the P25 electrode shows the highest signal of all electrodes. The signal rises up steeply above 0.004 V and saturates to a value of about 69.5 pA at 0.35 V. The CO_2 evolution of the TiO_2−C1a and TiO_2−C1b electrodes starts at higher voltages 0.08 V/NHE and 0.05 V/NHE, respectively, and saturates to values of about 4.1 pA and 8.3 pA above 0.4

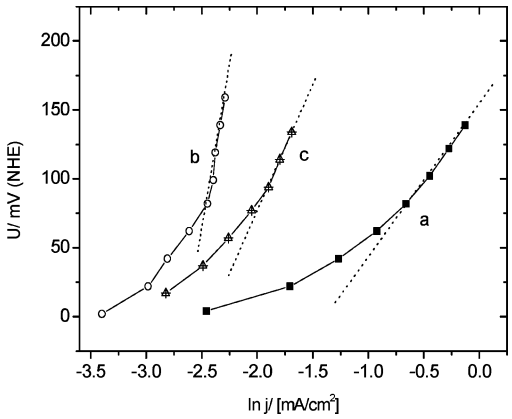

Figure 7. Tafel-plot of the different TiO_2 electrodes. The observed photocurrent density in formic acid oxidation (UV-light) is plotted versus the applied voltage (NHE). (a) P25; (b) TiO_2−C1a; (c) TiO_2−C1b.

V/NHE. The mass signal observed under Vis-light illumination is very low and equal for both C-doped electrodes (TiO_2−C1a/TiO_2−C1b 1.5 pA, 0.4 V). The value of photocurrent of the TiO_2−C1a electrode observed under Vis-light obviously could not be converted for the benefit of enhancing the oxidation of formic acid under UV-light. It is important to mention here that the oxidation of formic acid is a one-electron (defect electron) reaction, resulting in a higher product formation in relation to the current with respect to the watersplitting reaction.

The herein-estimated tafel slopes between undoped and doped TiO_2 are quite different for the formic acid oxidation. In Figure 7 the applied potential is plotted versus the natural logarithm of the current density and the tafel-slopes are presented as dotted lines. According to the formal Tafel equation (anodic, (1)[21]):

$$\ln j_D = \ln j_0 + \frac{\alpha n F}{RT}\eta_D \qquad (1)$$

where j_D is the main current density, j_0 is the exchange current density, n is the number of transferred electrons, α = transfer coefficient, F = Faraday constant ($9.648 \cdot 10^4$ C·mol^{-1}), R = ideal gas-constant (8.314 J·K^{-1}), T = temperature (298.15 K), and η_D is the applied potential; the following parameters were estimated. The slope for the P25-electrode is about 95 mV/decade and for the two carbon-doped electrodes the slopes are about 160 mV/decade (TiO_2−C1b) and 450 mV/decade (TiO_2−C1a) (Figure 7).

The steeper rise of the slope for the carbon-doped TiO_2 electrodes indicates a strongly changed reactivity of the surface, present the in form of a lower exchange current density, too.

Finally, measurements from carbon-doped TiO_2 electrodes, mixed with certain amounts of rutile, were prepared and investigated. This experiment was expected to confirm that no failure occurs during the preparation of electrodes and that all observed findings belong solely to the C−TiO_2 powder. Figure 8a compares the photocurrent observed for the oxidation of formic acid.

The current sets on at lower voltage (−0.08 V, 0.08 mA/cm^2) for the rutile-containing electrode (15 m%), and saturates to a higher value about 0.21 mA/cm^2 above 0.29 V. The CO_2 mass signal in Figure 8b increases from 4.1 pA for the TiO_2−C1a electrode (0.35 V) to a value of 6.5 pA for the TiO_2−C1a/rutile electrode (0.35 V). In general, the properties converge to the redox behavior of P25.

(b) Discussion of the Electrochemical Results. Let us consider the I−U characteristic of the doped and undoped TiO_2 electrodes

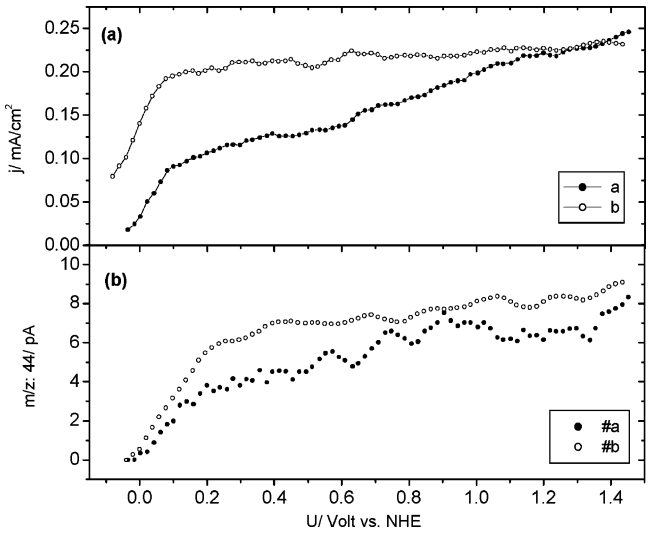

Figure 8. (a) Current−voltage characteristic of a pure TiO_2−C1a and a 15 m% rutile/TiO_2−C1a electrode (UV-light, 1 M HCOOH): (a) Pure TiO_2−C1a; (b) TiO_2−C1a/15 m% rutile. (b) Corresponding mass signal of carbon dioxide: (a#) pure TiO_2−C1a; (b#) TiO_2−C1a/15 m% rutile.

in acidic aqueous solution (Figure 3). The shape of the anodic photocurrent curve of the P25 electrode presents a typical *n*-type semiconductor behavior under illumination. The photogenerated holes move toward the surface (in the VB) and the electrons (in the CB) move toward the bulk. The saturation of the current at potentials above 0.3 V/NHE results mostly from the limitation of photogeneration and the limited electron transport to the back-contact. It reflects the general properties of the semiconductor/electrolyte interface of nanostructured electrodes.[22]

The apparent cathodic currents (only for P25 electrodes) were absent during cyclovoltammetry measurements (CV) in "non-contact" mode between electrode and membrane of the mass spectrometer. Therefore it is assumed that a limited release of oxygen favors its reduction at the electrode surface.

The carbon-doped electrodes TiO_2−C1a and TiO_2−C1b show more than 10-fold decreased photocurrent (Figure 3) and no measurable oxygen liberation with respect to the undoped TiO_2 electrode. It is assumed that the observed marginal photocurrents ($\sim$30 μA/cm^2) result from the behavior of the electrode as capacitor caused by trap filling processes as well as corrosion take part. Lindquist studied such trap filling processes for anatase and estimated similar values.[23] Surface defects (traps) at the C−TiO_2 electrodes should be present in a high quantity, because the partial oxidation of carbon during the annealing led to a strong reducing atmosphere. These defects can be electrochemically oxidized or reduced. This assumption is supported by the observation of decreasing photocurrents (>50%) after several solely anodic scans (8 scans). These carbon-doped electrodes bleached out and the subsequent complete CV-scan showed increased cathodic- and thereafter anodic-currents but without an increased oxygen evolution (UV-light). This suggests that the surface is changed dramatically and internal reactions occurred. One might consider that most of O_2 is photoevolved near the SnO_2/TiO_2 interface (backside illumination) and that partial re-reduction of O_2 reduces the photocurrent and the O_2-mass signal. But it has to be pointed out that for this reason thin films are used and that this undesired side-reaction appears at undoped TiO_2 as well. It is here much more pronounced, as apparent in the cathodic current after a complete CV scan. A high amount of adsorbed O_2 at the C−TiO_2/SnO_2 interface

should result in observable cathodic currents in the CV (−0.1 to +1.4 V/NHE). But they were not observed for the C−TiO_2 electrodes.

Adsorption and oxidation of formic acid at titanium dioxide has been described by Dulay and Anderson.[24] The increased photocurrent, especially for the P25 sample (Figure 5), is attributed to improved oxidation kinetics (one step reaction), the injection of an electron from the formic acid radical cation into the conduction band of the TiO_2, and the favorable involvement of water-oxidation intermediates such as the OH radical. Bogdanoff et al. even found an acceleration of the decomposition of formic acid after reaching the watersplitting onset potential,[25] supporting the involvement of intermediate radicals.

The carbon-doped TiO_2 electrodes show for the formic acid oxidation in general a similar current−voltage characteristic like the P25 electrode, but the slope, the maximum of current, and the mass signal are small with respect to P25-films (Figures 5 and 6). The values decrease with higher content of carbon (UV-light). Altogether the current and the detected CO_2 signals are smaller by a factor of 8 as compared to P25.

From the results observed, it is concluded that in acidic media the oxidation of formic acid at carbon-doped titanium dioxide does not occur any longer under participation of intermediates of water oxidation reaction (e.g., hydroxyl radicals). This conclusion is supported by the observation of a strongly diminished carbon dioxide signal upon illuminating with UV- and visible light, the failure of oxygen evolution in aqueous solution, the different Tafel-slopes, and the absence of the acceleration of the HCOOH oxidation after reaching the watersplitting potential (unlike in undoped TiO_2).

The Tafel slope estimated for the P25 electrode (Figure 7) was about 95 mV/dec and that for the carbon doped ones was 160 mV/dec (TiO_2−C1b) and 450 mV/dec (TiO_2−C1a). According eq 1, the slope is directly influenced by the transfer coefficient, the temperature (kept constant), and the number of transferred electrons. To describe the differences of the slopes, the transfer coefficient has to be changed or the number of transferred electrons differs. The last point should be excluded, therefore the estimated transfer coefficient α decreases from 0.26 TiO_2−P25 to 0.15 (TiO_2−C1b) and 0.05 (TiO_2−C1a). Using eq 2:[21]

$$\Delta G^*_+(\varphi_1) = \Delta G^*_+(\varphi_0) - \alpha n F \Delta\varphi \qquad (2)$$

where ΔG^* is the free activation enthalpie (anodic reaction), α is the transfer coefficient, n is the number of transferred electrons, F is the Farraday constant, and $\Delta\varphi$ is the positive changed potential, a weaker change of the free activation enthalpy for the carbon-doped electrodes can be deduced and therefore a lowered anodic reactivity related to the undoped material results.

To explain the low photocurrents (UV) of the carbon-doped electrodes, the missing oxygen liberation as well as the weak formic acid oxidation, with respect to the undoped material, the following model has to be taken into consideration.

Recent calculations on carbon-doped TiO_2 indicate that the new electronic states are located 1.1−1.25 eV above the valence band edge,[1] which is in agreement with the onset of light absorption in Figure 2 (1.41 eV) and with spectral photovoltage measurements in Figure 10a. It is proposed that the oxidation of formic acid observed in the experiments before takes place at these carbon-states. After excitation with energies above 3.2 eV, the photogenerated holes from the O-2p valence band edge are apparently relaxing fast into these new defect states without

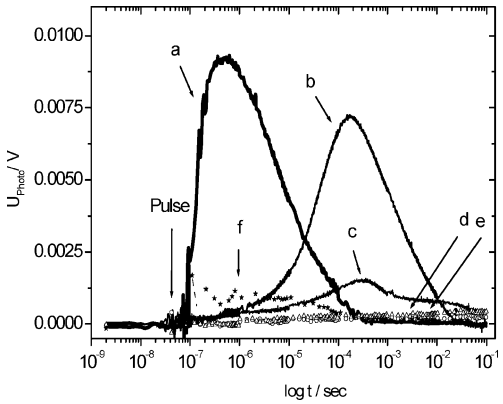

Figure 9. Photovoltage transients for different TiO_2 electrodes (excitation 337 nm pulse). (a) P25, well-equilibriated 3 days in air; (b) P25, semi-equilibriated 1 day in air; (c) P25, not equilibriated 20 min in air; (d) TiO_2−C1a, 3 days; (e) TiO_2−C1b, 3 days; (f) TiO_2−C1a/rutile.

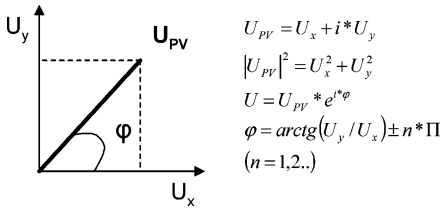

Figure 10. Presentation of the PV signal on a complex pain.[19b]

initiation of oxygen evolution. The photoexcited electrons in the conduction band are apparently not able to reach the back-contact to contribute to a high anodic current and they cannot induce an indirect dissociation of water (via OH-radical-anions and hydrogen peroxide). More information about this last process in N−TiO_2 has been published by Nakato recently.[25b] Using sub-bandgap excitation (<3.0 eV), the formic acid will be oxidized as well (Figures 5 and 6), but the generation of holes is restricted for excitation from defect states between the band gap, and further their quantity is lower due to the weaker illumination intensity. This causes the much lower rate (CO_2 signal: Vis-light, 1.5 pA; UV-light, 8.3 pA). It can be summarized that obviously the holes trapped at these C-midgap states can oxidize organic material only and they cannot induce oxygen evolution, neither under UV-light nor under Vis-light. The oxidizing properties of the carbon-doped TiO_2 are disadvantageous during illumination with UV-light in comparison to undoped titanium dioxide. A similarly diminished photocatalytic activity is reported by Itoh.[26] The decomposition of methylene blue declined sharply above a carbon-ion dose of 10^{14} ions/cm^2. Recently, Hoffmann et al. published a failure of OH-radical production under Vis-light illumination for N-doped TiO_2.[27] Tachikawa et al. examined the oxidation power of pure, and S- and C-doped TiO_2 powders in using 4(methylthio)-phenyl-methanol.[27b] The one electron oxidation ability of the C−TiO_2 is again substantially lower than that of pure TiO_2. Further, it is shown that a large amount of holes are trapped in the particle itself and not at the surface, which is in perfect agreement with the results from spectral resolved surface photovoltage measurements (SPV) hereinafter described.

Surface Photovoltage Measurements in Air (SPV). Spectral and time-resolved capacitive surface photovoltage measurements (SPV)[19] were performed with identical electrode compositions such as in the electrochemical measurement. SPV measurements are based on monitoring illumination-induced changes in the surface potential, as a function of incident photon energy (spectral PV) or as a function of time (transient measurements).

Once the electrodes were measured immediately after the annealing (so-called unequilibriated), some were equilibrated for various time periods (2 and 3 days). Additionally, the carbon-doped electrodes were subjected to prolonged firing, to find whether they could be converted to undoped titania through air oxidation.

Figure 9 shows the time-resolved PV measurements for P25 and carbon-doped TiO_2 samples. The most significant feature of a PV transient is a pronounced peak with a characteristic time (t_{peak}) and amplitude (PV_{peak}). Comparing the transients of the different TiO_2−P25 electrodes, an apparent correlation of PV_{peak} and t_{peak} with the presence of adsorbed water is observed. The well-air-equilibrated P25 sample (a) shows a positive PV signal which rapidly increases immediately after the laser pulse. The value of PV_{peak} is about 9 mV and the value of t_{peak} is $5 \cdot 10^{-7}$ s.

With decreasing time of equilibration in air, PV_{peak} decreases from 9.2 mV (3 days, Figure 9a) to 7.1 mV (1 day, Figure 9b), and finally to 1.5 mV (30 min, Figure 9c), whereas the value of t_{peak} increases from $5 \cdot 10^{-7}$ to $1.7 \cdot 10^{-4}$ s, to finally $3.3 \cdot 10^{-4}$ s. None of the carbon-doped TiO_2 samples (TiO_2−C1a, TiO_2−C1b) showed a PV transient signal, neither under equilibration within 3 days nor for 30 min. Upon increasing the annealing time from 6 min to 1 h at 350 °C, the sample became colorless but did not produce a PV signal. Only the TiO_2−C1a/Rutile electrode (f) shows a signal of low intensity (PV_{peak} 1.5 mV, t_{peak} 2×10^{-6} s).

Stationary, spectral photovoltage measurements are more sensitive due to the possible longer integration time for the signal. In Figure 10 the relation of the photovoltage amplitude U_{PV} to the co-phased (U_x) and phase shifted U_y (by 2Π, with respect to the chopped light) signal are presented.

In Figure 11a, the PV amplitude (PV_{max}) is presented. The signal of the P25 electrode sets on above excitation energies of 3.0 eV, corresponding to the band gap energies of rutile and anatase (3.0 and 3.2 eV). The apparent decline of the signal at energies above 3.5 eV results mainly from increased recombination under strong absorption conditions. The air-equilibrated P25 sample did not show signals at energies below the band gap, indicating that there are no energetic states below the conduction band. The signal of both carbon-doped TiO_2 electrodes sets in at a value of 1.9 eV already. The curve is shaped like a plateau, rather than a peak as observed for the P25 electrode. Surprisingly, the TiO_2−C1a and TiO_2−C1b electrodes did not show a strong increase of the signal related to the TiO_2 band to band absorption.

However, this result is in agreement with the time-resolved measurements. A TiO_2−C1a electrode, which was annealed for 1 h instead of 6 min, shows a lowered value of PVmax (6 min, 0.016 mV; 1 h, 0.007 mV at 2.2 eV), but like the other carbon-doped TiO_2 electrodes shows no strong TiO_2 band to band absorption. The electrode containing 15 m% rutile (10, d) shows only a PV signal for excitation above 3.0 eV.

The onset of the photovoltage at energies much below the band gap is caused by deep defect states in the band gap. Defect states can be generated through reduction reactions, introduced dopant-ions, or from vacuum annealing.

The phase angle (Figure 11, explanation Figure 10) results from the correlation between the in-phase and phase-shifted PV signal and it gives information about the charge separation mechanism. When the sign of the in-phase photovoltage signal changes from positive to negative, the phase angle becomes negative, too. It can then be deduced that the dominating charge trapping mechanism at the surface has changed. At the P25

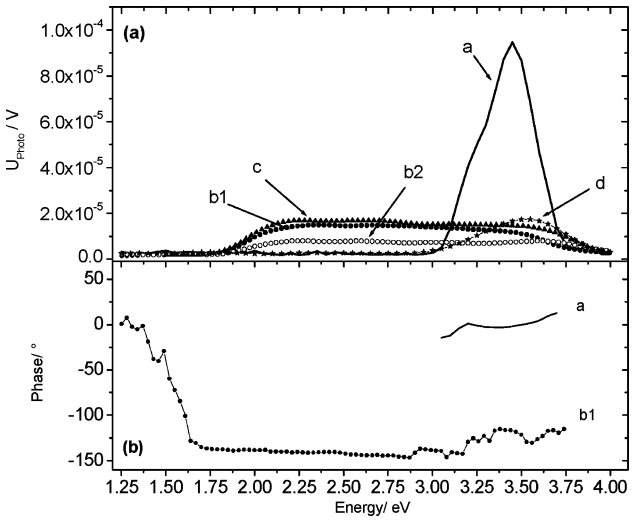

Figure 11. (a) Spectral photovoltage measurement: (a) P25; (b1) TiO_2−C1a, 6 min + 350 °C annealing; (b2) TiO_2−C1a, 1 h + 350 °C annealing; (c) TiO_2−C1b (6 min + 350 °C); (d) TiO_2−C1a + 15 m% rutile (6 min + 350 °C). (b) Phase shift between the U_x and U_y voltage signal, resulting from the in-phase and cophase lock-in amplifier signal: (a) P25, no phase shift; (b) TiO_2−C1a, phase shift of about 150°.

electrode the photoinduced electrons move toward the back-contact and holes move toward the surface. For the TiO_2−C1a electrode this behavior is opposite.

In the following section, the results from PV measurements will be summarized and discussed. Water ambience strongly influences the surface photovoltage of P25 electrodes. In transient measurements PV_{peak} increases and t_{peak} decreases with increasing amount of water.

The strong change of t_{peak} (>2 magnitudes) indicates a major change in conductivity in water atmosphere. This is supported by the investigation of a humidity-dependent surface conductivity of TiO_2 electrodes, measured with impedance technique.[28] Carbon-doped TiO_2 electrodes show no transient signal, neither equillibriated nor after annealing for 1 h at 350 °C. It is supposed that the absence of a PV signal results either from a recombination faster than 5 ns or from the absence of an efficient charge-trap at the surface. Water from humid air is obviously not able to interact with the surface.

In spectral measurements, the P25 electrode equilibriated in air shows no PV signal below band gap energies, whereas all carbon-doped electrodes do. From this the existence of defect states in the band gap can be deduced. Further, it is noted that these states are apparently not influenced by the presence of water. The sign of the in-phase PV signal gives information about the charge separation mechanism. The charge separation mechanism of the carbon-doped electrodes is opposed to that of P25: photogenerated electrons and holes move to the surface and bulk, respectively. Water cannot function as a crucial hole-trap for the C-doped electrodes.

To point out that the PV signal is strongly influenced by the presence of qualified reactants (trapping of charge carrier) additional measurements were done with formic acid. Figure 12 shows the PV amplitude correlated with the excitation energy for the doped and undoped electrodes. For a better comparison the spectra of the electrodes without formic acid are introduced as well. The signal of the P25 electrode sets on at 2.4 eV already and increases by the factor of 2 compared to the P25 electrode without formic acid. Furthermore, the PV maximum shifts from 3.5 to 3.7 eV indicating a decreased charge-recombination. The

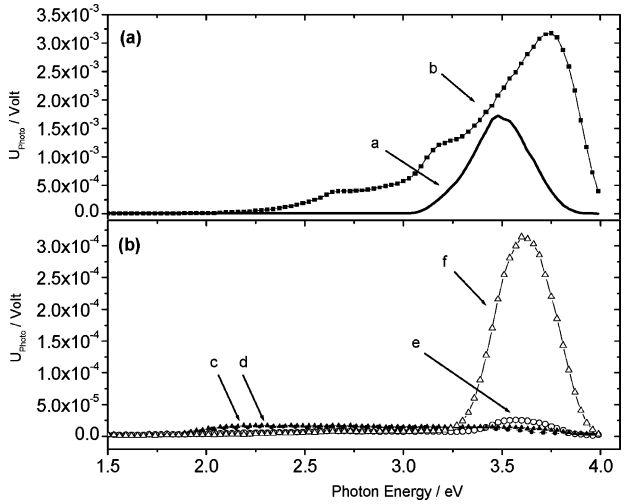

Figure 12. Spectral PV measurement in the presence of formic acid sprinkled on to the electrodes. (a) Pure P25; (b) P25 and HCOOH; (c) TiO_2−C1a, pure; (d) TiO_2−C1b, pure; (e) TiO_2−C1a, with HCOOH; (f) TiO_2−C1b, with HCOOH. Note the change of the power between P25 and the TiO_2−C.

presence of formic acid led the photovoltage of the TiO_2−C1a and TiO_2−C1b electrodes to increase too.

Where the value of the PV maximum rises slowly for TiO_2−C1a (from 0.013 to 0.025 mV at 3.5 eV), it grows more strongly for the TiO_2−C1b electrode (from 0.014 to 0.31 mV at 3.5 eV). The sample with the lower content of carbon shows again a higher reactivity. Surprisingly, the photovoltage for TiO_2−C1b increases 10-fold with respect to that of TiO_2−C1a but the increase of photocurrent was only 2-fold. For some explanation, it is important to mention that already a charge separation of some nanometers led to a measurable photovoltage but this separation cannot be generalized to kinetics of a complete redox-reaction as would be measured with (wet) electrochemistry. At least the signals are 1 order of magnitude lower than those of P25. The appearance of an enhanced PV signal after band to band excitation indicates the possibility for trapping holes at the upper edge of the valence band with qualified reactants. Because of the limitation of these effects to the presence of formic acid, it is assumed that the relaxation of the holes from the upper edge of the valence band to the defect states in the band gap is too fast for initiation of a surface OH-radical- or titanium peroxide-intermediates (e.g., Ti−O−O−Ti) with a subsequent water splitting reaction.

Consequences for the Mechanism of Water Cleavage. As shown in the previous sections the photooxidation of water is inhibited at the carbon-doped samples, whereas it proceeds at undoped P25. The process of water oxidation at anatase has been discussed for three decades resulting in various mechanisms.[29,30] Whereas the involvement of an OH-radical is controversially discussed,[31−34] other oxygen-based radicals are commonly invoked as intermediates. Recently, major progress in understanding has been achieved. On the basis of isotopic experiments (^{18}O), IR-spectroscopic identification of peroxo-intermediates, and photoluminescence measurements, Nakato et al. postulated a "nucleophilic attack mechanism" as schematically depicted in Scheme 1.[35] The characteristic emission band at 840 nm (1.48 eV) was assigned to the recombination of conduction band electrons with surface trapped holes at the bottom of atomic grooves at the (100) face. In the case of water oxidation these holes are supposed to be involved in the first reaction step together with the simultaneous nucleophilic attack of a water molecule at an oxo-bridged titanium center resulting

SCHEME 1: Watersplitting Mechanism Published by Nakato et al[35]

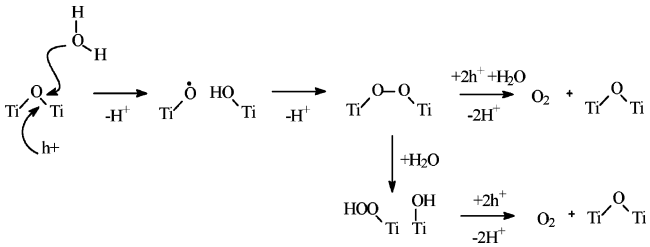

SCHEME 2: Modified Watersplitting Mechanism

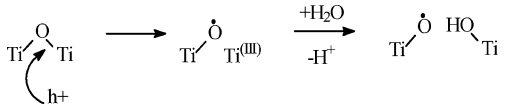

in Ti−O bond cleavage and forming of a titanyl radical and a hydroxo-titanium species.

Dimerization of the titanyl radical leads to a peroxo complex which is further oxidized to oxygen under reformation of the oxo-bridged titanium center. The most important aspect of this mechanism is the fact that the first step is supposed to occur from holes trapped at 1.48 eV (840 nm) below the conduction band edge, corresponding to a redox potential of about 1.34 V (see TiO_2 band edges in Figure 1). One therefore would expect that these states should have been detectable in our photovoltage and oxygen measurements. Since this was not the case, the proposed mechanism has to be modified. From all experimental findings presented above, it follows that oxygen evolution occurs only when a hole can be generated at the upper end of the valence band. We therefore propose a modified mechanism (Scheme 2). The first step results in the initial formation of a radical cation due to the trapping of a hole and a Ti−O−Ti bond-breaking (O-2p valence band edge, ∼3.06 eV/NHE). The following attack of a water molecule leads to the formation the same titanyl- and hydroxotitanium-species as suggested in the previous mechanism (Scheme 1).

A further argument underlining that oxygen evolution is unlikely to occur via a trapped hole located at about 1.34 V is the following. Considering that the hydrogen potential ($E°_{H_2/H+}$) is also situated 0.14 eV below the conduction band edge (Figure 2), it follows that the holes are located in the region of the 4-electron oxidation potential for water cleavage ($E°_{(O_2/H_2O)}$ 1.23 V NHE, pH 0). Taking into account that the reaction corresponds to a 4-electron reaction and that the first one-electron oxidation step of water can never approach such an ideal value, it must be concluded that the photoluminescence arises from a second or subsequent hole, which is involved in formation and transformation of the titaniumperoxo complexes. The modified reaction pathway (Scheme 2) obviously requires the initiation of water-splitting p-states of oxygen.

They cannot be replaced by energetically similar positioned states of a different nature, because a surface bonded radical oxygen state is required. This conclusion is entirely supported by the capacitive photovoltage measurements of the doped and undoped TiO_2 samples, which show that in the carbon-doped materials the photoactivity from the O-2p states (E_G > 3.2 eV) breaks down (Figures 9 and 10). In presence of water, the holes apparently relax rapidly into higher positioned gap states. The absent correlation of the PV signal with the amount of water led to the conclusion of a failed interaction with water molecules (Figure 9). Only oxidation of organic compounds can proceed (Figures 4 and 10, no interaction with H_2O; Figures 6 and 11, interaction with organic material).

Studies similar to those with the carbon-doped TiO_2 were also performed in our laboratory with a limited number of nitrogen-doped TiO_2 ($N-TiO_2$) samples. These were sputtered TiO_2 layers containing different concentrations of nitrogen[36] as well as chemically prepared N-doped TiO_2.[11b] In all investigated cases they show basically the same results as the carbon-doped samples.

Conclusion

All together, according to our experiments, it has to be stated that carbon doping cannot extend oxygen evolution toward the visible spectral region. It even drastically reduces the oxygen evolution activity within the UV-region. Capacitive photovoltage measurements and electrochemical mass spectroscopy confirm that the relaxation of holes into defect states located in the band gap is too fast for efficiently inducing an interfacial water oxidation. Only organic compounds such as formic acid, which involve one-electron-transfer processes, can be oxidized. The strong decreased activity (oxygen evolution) of the carbon-doped TiO_2 electrodes makes their use in their present material quality and as thin film electrodes difficult. Due to their lack of reactivity with water, carbon-doped TiO_2 is an unlikely candidate for vis-light induced super-hydrophilicity, which appears to be in agreement with ref 37.

As a consequence, on the basis of our studies, it is difficult to understand reports on efficient visible light water splitting, using this type of material, as reported elsewhere.[7]

Acknowledgment. We thank Dr. Th. Dittrich for support with the PV-measurements and for the stimulating discussions.

References and Notes

(1) Asahi, R.; Morikawa, T.; Ohwaki, T.; Aoki, K.; Taga, Y. *Science* **2001**, *293*, 269.

(2) (a) Sakthivel, S.; Kisch, H. *ChemPhysChem* **2003**, *4*, 487. (b) Irie, H.; Watanabe, Y.; Hashimoto, K. *J. Phys. Chem. B* **2003**, *107*, 5483.

(3) Lindgren, T.; Mwabora, J. M.; Avendano, E.; Jansson, J.; Hoel, A.; Granqvist, C.-G.; Lindquist, S.-E. *J. Phys. Chem. B* **2003**, *107*, 5709.

(4) Irie, H.; Watanebe, Y.; Hashimoto, K. *J. Phys. Chem. B* **2003**, *107*, 5483.

(5) Irie, H.; et al. *Chem. Commun.* **2003**, *11*, 1298.

(6) (a) Sakthivel, S.; Kisch, H. *Angew. Chem.* **2003**, *115*, 5057. (b) Sakthivel, S.; Janczarek, M.; Kisch, H. *J. Phys. Chem. B* **2004**, *108*, 19384.

(7) Khan, S. U. M.; Al-Shahry, M.; Ingler, W. B., Jr. *Science* **2002**, *297*, 2243.

(8) Irie, H.; et al. *Chem. Lett.* **2003**, *32*, 772.

(9) Umebayashi, T.; et al. *Appl. Phys. Lett.* **2002**, *81*, 454.

(10) Umebayashi, T.; et al. *Appl. Phys. Lett.* **2003**, *32*, 330.

(11) (a) Ohno, T.; et al. *Chem. Lett.* **2003**, *32*, 364. (b) Sakthivel, S.; Janczarek, M.; Kisch, H. *J. Phys. Chem. B* **2004**, *108*, 19384.

(12) (a) Hoffmann, M. R.; Martin, S. T.; Choi, W.; Bahnemann, D. W. *Chem. Rev.* **1995**, *95*, 69. (b) Ollis, D. F.; Al-Ekabi, H. *Photocatalytic Purification and Treatment of Water and Air*; Elsevier: Amsterdam, 1993.

(13) Bak, T.; Nowotny, J.; Rekas, M.; Sorell, C. C. *Int. J. Hydrogen Energy* **2002**, *27*, 991.

(14) (a) Ihara, T.; Miyoshi, M.; Iriyama, Y.; Matsumoto, O.; Sughihara, S. *Appl. Catal., B* **2003**, *42*, 403. (b) Ohno, T.; Tsubota, T.; Nishijima, K.; Miyamoto. Z. *Chem. Lett.* **2004**, *33*, 750. (c) Irie, H.; Watanabe, Y.; Hashimoto, K. *J. Phys. Chem. B* **2003**, *107*, 5483.

(15) Kato, H.; Kudo, A. *J. Phys. Chem. B* **2002**, *106*, 5029.

(16) Ishikawa, A.; Takata, T.; Kondo, J. N.; Hara, M.; Kobayaski, H.; Domen, K. *J. Am. Chem. Soc.* **2002**, *124*, 13547.

(17) Estimation of U_{fB} with the suspension-method: Roy, A. M.; De, G. C.; Samsal, N.; Bhattacharyya, S. S. *Int. J. Hydrogen Energy* **1995**, *20*, 627.

(18) Bogdanoff, P.; Alonso-Vante, N. *Ber. Bunsen-Ges. Phys. Chem.* **1993**, *97*, 940.

(19) (a) Duzhko, V.; Timoshenko, V. Y.; Koch, F.; Dittrich, T. *Phys. Rev. B* **2001**, *64*, 075204. (b) Duzhko, V. Photovoltage Phenomena in nanoscale materials, Dissertatiokn, TU-München, 2002.

(20) Scherrer eq: $d = 7.95/[(\text{fwhm}\wedge 2 - 0.001\wedge 2)\cos\Theta]$, where fwhm is the full width of peak at the half-maximum; Θ is the Bragg angle; 7.95 is an estimated apparatus constant with incident wavelength (Cu Kα) and Scherrer quotient.

(21) Hamann, C. H.; Vielstich, W. *Elektrochemie;* Wiley VCH: Weinheim, 1998.

(22) Lindström, H.; Rensmo, H.; Södergren, S.; Solbrand, A.; Lindquist, S. E. *J. Phys. Chem.* **1996**, *100*, 3084.

(23) Wang, H.; He, J.; Boschloo, G.; Lindström, H.; Hagfeldt, A.; Lindquist, S. E. *J. Phys. Chem. B* **2001**, *105*, 2529.

(24) (a) Fox, M. A.; Dulay, M. T. *Chem. Rev.* **1993**, *93*, 341. (b) Aguado, M. A.; Anderson, M. A. *Solar Energy Mater. Solar Cells* **1993**, *28*, 345.

(25) (a) Bogdanoff, P.; Alonso-Vante, N. *J. Electroanal. Chem.* **1994**, *379*, 415. (b) Nakamura, R.; Tanaka, T.; Nakato, Y. *J. Phys. Chem. B* **2004**, *108*, 10617.

(26) Choi, Y.; Yamamoto, S.; Itoh, H. *NIM B* **2003**, *206*, 241.

(27) (a) Mrowetz, M.; Balcerski, W.; Colussi, A. J.; Hoffmann, M. R. *J. Phys. Chem. B* **2004**, *108*, 17269. (b) Tachikawa, T.; Tojo, S.; Kaway, K.; Endo, M.; Fujitsuka, M.; Ohno, T.; Nishijima, K.; Miyamoto, Z.; Majima, T. *J. Phys. Chem. B* **2004**, *108*, 19299.

(28) Garcia-Belmonte, G.; Kytin, V.; Dittrich, T.; Bisquert, J. *J. Appl Phys.* **2003**, *94*, 5261.

(29) (a) Wilson, R. H. *J. Electrochem. Soc.* **1980**, *127*, 228. (b) Salvador, P.; Gutierrez, C. *J. Phys. Chem.* **1984**, *88*, 3696.

(30) (a) Nakamura, R.; Imanishi, A.; Murakoshi, K.; Nakato, Y. *J. Am. Chem. Soc.* **2003**, *125*, 7443. (b) Jaeger, C. D.; Bard, A. J. *J. Phys. Chem.* **1979**, *83*, 3146.

(31) Schwarz, F. P.; Turro, J. N.; Bossmann, S. H.; Braun, A. M.; Wahab, A.; Dürr, H. J. *J. Phys. Chem. B* **1997**, *101*, 7127.

(32) Anpo, M.; Shima, T.; Kubokawa, Y. *Chem. Lett.* **1985**, 1799.

(33) Micic, O. I.; Zhang, Y.; Cromack, K. R.; Trifunac, A. D.; Thurnauer, C. M. *J. Phys. Chem.* **1993**, *97*, 7277.

(34) Fan, J.; Yates, T. J. *J. Am. Chem. Soc.* **1996**, *118*, 4686.

(35) Nakamura, R.; Nakato, Y. *J. Am. Chem. Soc.* **2004**, *126*, 1290.

(36) Koslowski, U.; Ellmer, K. *J. Appl. Phys*., submitted for publication.

(37) Irie, H.; Washizuka, S.; Hashimoto, K. *IPS-15*, 2004, oral session (W6-O-10).